

Supplementary Information for Hicks et al. (Pharmacokinetic/pharmacodynamic modeling identifies SN30000 and SN29751 as tirapazamine analogs with improved tissue penetration and hypoxic cell killing in tumors)

Table of Contents

	Pg
Synthesis of SN30000	2
Table S1: Maximum tolerated dose of TPZ, SN29751 and SN30000 in mice and rats	3
Table S2: Histopathology of TPZ, SN29751 and SN30000 in CD-1 nude mice	4
Table S3: Plasma pharmacokinetics of i.p. and i.v. SN30000 in CD-1 nude mice	5
Table S4: Plasma pharmacokinetics of TPZ, SN 29751 and SN30000 in rats	6
Fig. S1: 1-oxide metabolite of SN30000 in extracellular medium of hypoxic HT29 cultures	7
Fig. S2: Flux of TPZ, SN29751 and SN30000 through SiHa multicellular layers	8
Fig. S3: Oxygen dependence of metabolism of TPZ, SN29751 and SN30000 in HT29 cell suspensions	9
Fig. S4: Retinal toxicity of TPZ, SN29751 and SN30000 in CD-1 nude mice	10
Fig. S5: SR-PKPD model predictions for TPZ, SN29751 and SN30000 for HT29 tumors in rats	11
Fig. S6: Lack of correlation between <i>in vitro</i> and <i>in vivo</i> cytotoxicity	12

Synthesis of SN30000

SN30000 was synthesized by the following modification of a method for tricyclic triazine dioxide synthesis (Hay MP, Hicks KO, Pchalek K, Lee HH, Blaser A, Pruijn FB *et al.* Tricyclic [1,2,4]triazine 1,4-dioxides as hypoxia selective cytotoxins. *J Med Chem* 2008;51:6853-568).

3-[3-(4-Morpholinyl)propyl]-7,8-dihydro-6H-indeno[5,6-*e*][1,2,4]triazine 1,4-dioxide.

Hydrogen peroxide (70%, 2.8 mL, ca. 56 mmol) was added dropwise to a stirred solution of trifluoroacetic acid (TFA) (7.9 mL, 56 mmol) in 20 mL dichloromethane (DCM) at 0 °C. The solution was stirred at 0 °C for 5 min, warmed to 20 °C for 10 min, then cooled to 0 °C. The solution was added to a solution of 3-[3-(4-morpholinyl)propyl]-7,8-dihydro-6H-indeno[5,6-*e*][1,2,4]triazine 1-oxide (1.76 g, 5.6 mmol) and TFA (2.2 mL, 28 mmol) in DCM (40 mL) at 0 °C and the solution was stirred at 20 °C for 4 h. Dilute aqueous ammonia solution (40 mL) was added and the mixture stirred vigorously for 30 min and then extracted with DCM (4 × 50 mL). The combined organic fraction was dried and the solvent evaporated. The residue was purified by chromatography, eluting with a gradient (0–10%) of methanol (MeOH)/DCM, to give (i) starting material (173 mg, 10%); and (ii) the 1,4-dioxide (868 mg, 47%) as a yellow solid: mp (MeOH/DCM) 109–110 °C; ¹H NMR δ 8.30 (s, 1 H, H-9), 8.27 (s, 1 H, H-5), 3.44 (br t, *J* = 4.4 Hz, 4 H, 2 × CH₂O), 3.24 (br t, *J* = 7.3 Hz, 2 H, CH₂), 3.13–3.19 (m, 4 H, H-6, H-8), 2.50 (t, *J* = 6.5 Hz, 2 H, CH₂N), 2.38 (br t, *J* = 4.3 Hz, 4 H, 2 × CH₂N), 2.27 (p, *J* = 7.5 Hz, 2 H, H-7), 2.06–2.12 (m, 2 H, CH₂); ¹³C NMR δ 155.2, 155.1, 150.5, 139.0, 133.7, 115.8, 113.8, 67.0 (2), 58.0, 53.5 (2), 33.3, 32.8, 28.5, 25.5, 21.8. Anal. calcd for C₁₇H₂₂N₄O₃: C, 61.8; H, 6.7; N, 17.0. Found: C, 62.0; H, 6.8; N, 17.2%.

The compound was formulated as the HCl salt: 3-[3-(4-morpholinyl)propyl]-7,8-dihydro-6H-indeno[5,6-*e*][1,2,4]triazine 1,4-dioxide hydrochloride.

A solution of HCl in MeOH (1.25 M, 2.3 mL, 2.9 mmol) was added to a solution of 1,4-dioxide (0.85 g, 2.6 mmol) in MeOH (5 mL) and DCM (5 mL). The solvent was evaporated, MeOH (5 mL) added and the solvent evaporated and the residue dried under vacuum. The hydrochloride salt was recrystallized from MeOH/ethyl acetate to give 1,4-dioxide·HCl (0.85 g, 90%) as a pale yellow solid: mp (MeOH/ethyl acetate) 161–163 °C; ¹H NMR [(CD₃)₂SO] δ 10.10 (br s, 1 H, NH⁺Cl⁻), 8.22 (s, 2 H, H-5, H-9), 3.93–4.00 (m, 2 H, CH₂O), 3.67–3.75 (m, 2 H, CH₂O), 3.21–3.28 (m, 6 H, H-6, H-8, CH₂), 3.02–3.17 (m, 6 H, 3 × CH₂N), 2.18–2.25 (m, 2 H, CH₂), 2.15 (pent, *J* = 7.5 Hz, 2 H, H-7); ¹³C NMR [(CD₃)₂SO] δ 154.5, 152.5, 150.2, 138.7, 133.7, 115.2, 113.1, 63.2 (2), 55.1, 51.0 (2), 32.7, 32.2, 26.9, 25.2, 18.7. Anal. calcd for C₁₇H₂₃ClN₄O₃: C, 55.7; H, 6.3; N, 15.3. Found: C, 55.7; H, 6.4; N, 15.2%. The purity of the HCl salt, measured by HPLC, was >98% (total wavelength chromatogram).

Supplementary Table S1 Maximum tolerated doses (MTD) after i.p. administration of TPZ, SN29751 and SN30000 in mice and rats.

Species	Strain	Sex	Schedule	MTD $\mu\text{mol/kg/dose}$ (mg/kg/dose , N ^a)		
				TPZ	SN29751	SN30000
Mouse	CD-1 nu/nu	Male	SD ^b	178 (31.7, 9)	1000 (370, 6)	750 (275, 9)
Mouse	CD-1 nu/nu	Male	BID 1-4 ^c	56.2, (10.0, 8)	421 (156, 9)	237 (86.9, 6)
Mouse	CD-1 nu/nu	Male	QD 4 ^d	133 (23.7, 6)	ND	420 (154, 6)
Mouse	Rag1 ^{-/-}	Male	SD	237 (42.2, 6)	562 (208, 3)	237 (86.9, 6)
Mouse	Rag1 ^{-/-}	Female	SD	ND	ND	237 (86.9, 6)
Mouse	C57/Bl6J	Male	SD	178 (31.7, 6)	750 (278, 3)	316 (117, 6)
Mouse	C3H/HeN	Female	SD	316 (56.3, 6)	750 (278, 3)	750 (275, 6)
Rat	Sprague Dawley	Male	SD	178 (31.7, 6)	421 (156,4)	316 (116,6)
Rat	Sprague Dawley	Female	SD	178 (31.7, 6)	316 (117,3)	316 (116,6)

^a Number of animals tested at the MTD dose level

^b Single dose

^c Bi-daily (9 am and 3 pm) \times 4

^d Daily \times 4

Supplementary Table S2. Histopathology in CD-1 nude mice after i.p. dosing with either single doses or BID1-4 (3M, 3F/group). Tissues assessed: small and large intestine, femoral bone marrow, liver, spleen, heart, lungs, kidneys.

Cmpd	Dose ($\mu\text{mol/kg}$)	Day	Mean wt loss	Significant findings
Control	-	-		None
TPZ	178	2	8.4%	GI toxicity BM hypoplasia Airway epithelial vacuolation
	237	1	11.2%	GI toxicity BM hypoplasia Airway epithelial vacuolation
SN29751	1000	2	2.4%	GI toxicity BM hypoplasia Airway epithelial vacuolation (Males only)
	1330	1	11.7%	2 deaths, 1 cull; Findings as above (M&F), plus 2/3 liver tox (moderate multifocal liver vacuolation in 2/3 males.
SN30000	750	2	9.5%	GI toxicity BM hypoplasia (femur and sternum) Airway epithelial vacuolation
TPZ	75 \times 8	5	11% in M, 6% in F	GI toxicity (large and small intestine, Paneth cell vacuolation, single cell necrosis, mucosal cell hypertrophy, increased mitoses)
SN29751	316 \times 8	5	-4% (gain)	GI toxicity, more severe in females BM hypoplasia (less than single dose) Airway epithelial vacuolation (Males only)
	421 \times 7	4	0.2%	1 death. Findings as above (males & females) with increased severity.
SN30000	237 \times 8	2	6.2%	GI toxicity. Airway epithelial vacuolation & bronchial epithelial necrosis in 1/3 F.

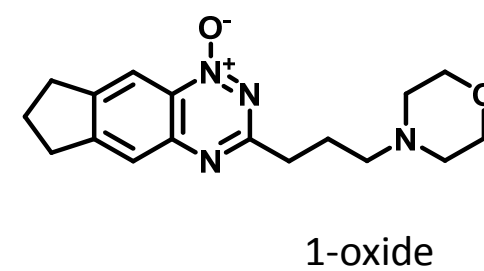
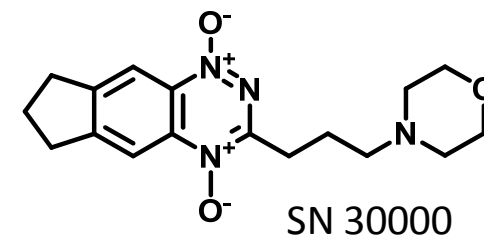
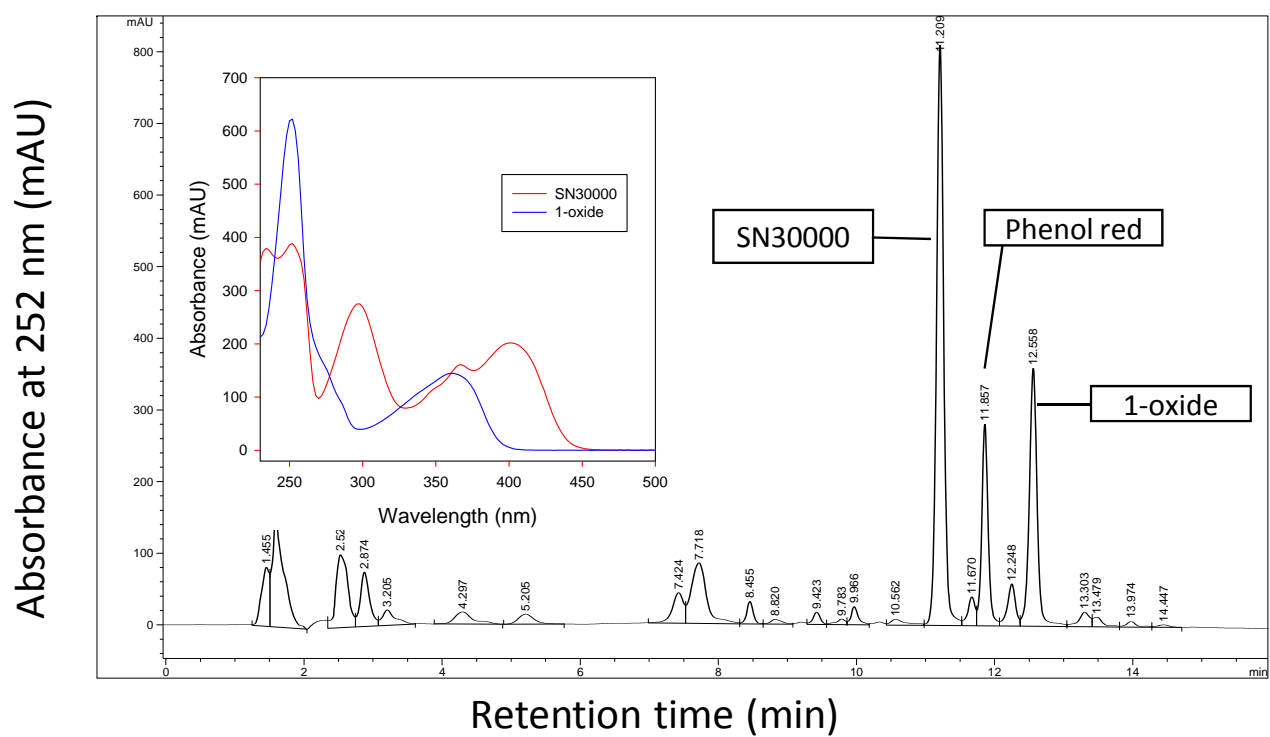
Supplementary Table S3: Pharmacokinetic parameters after i.p. or i.v. administration of SN30000 at 316 $\mu\text{mol/kg}$ to CD1 male nude mice in the same experiment (used for calculating the i.p. bioavailability of SN30000).

	i.v.	i.p.
$T_{1/2}$ (min)	24	23
C_{max} (μM) ^a	160 ± 10	122 ± 7
$\text{AUC}_{0-\infty}$, ($\mu\text{M}\cdot\text{hr}$)	80.7	62.2

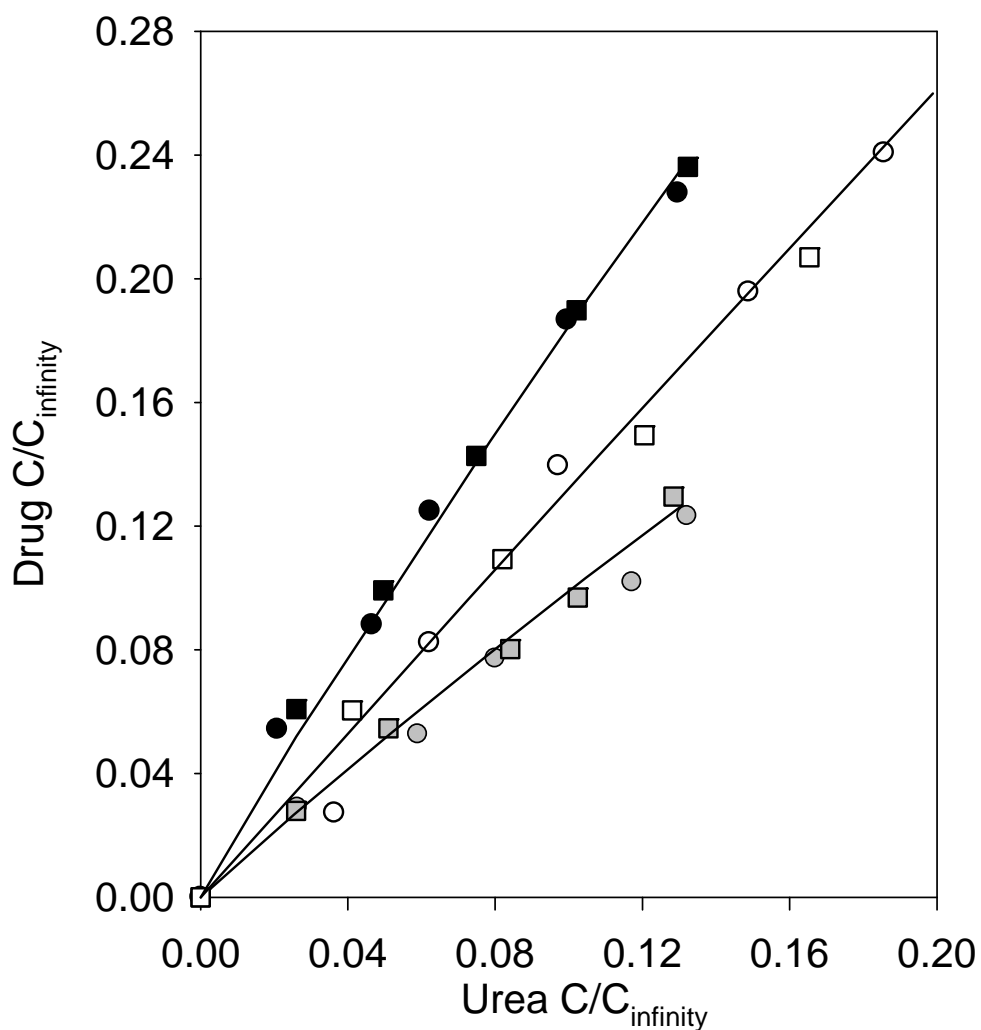
^aValues are mean and SEM.

Supplementary Table S4: Pharmacokinetics of TPZ, SN29751 and SN30000 in male and female Sprague-Dawley rats after i.p. administration. Mean \pm SEM, N=2 for all groups

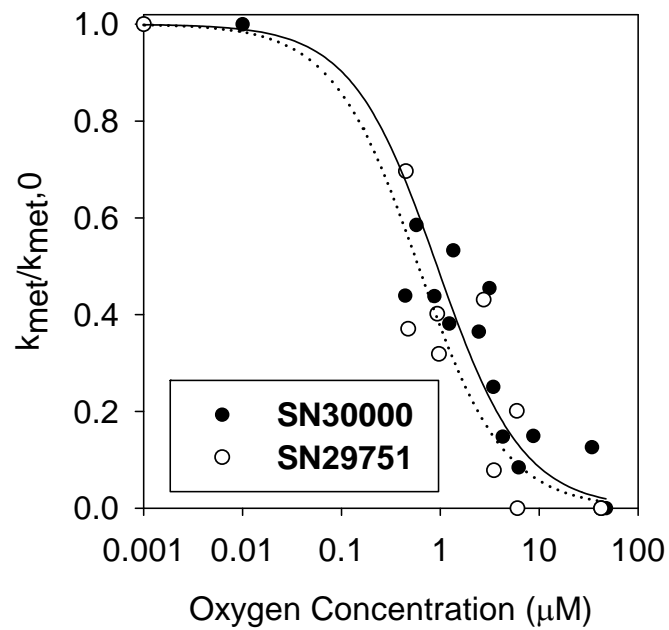
	TPZ		SN29751				SN30000			
Dose ($\mu\text{mol/kg}$)	178		178		316		178		316	
Sex	Male	Female	Male	Female	Male	Female	Male	Female	Male	Female
$T_{1/2}$, min	43 \pm 1	36 \pm 4	56 \pm 0	63 \pm 1	92 \pm 4	94 \pm 6	58 \pm 8	58 \pm 3	44 \pm 3	67 \pm 3
C_{max} , μM	80 \pm 1	95 \pm 2	103 \pm 6	116 \pm 3	202 \pm 16	203 \pm 8	49 \pm 4	83 \pm 2	112 \pm 5	183 \pm 8
$\text{AUC}_{0-\infty}$, $\mu\text{M}\cdot\text{hr}$	73.0 \pm 5.5	122.9 \pm 3.3	144.5 \pm 7.3	197.8 \pm 4.4	463.3 \pm 1.6	472.9 \pm 35.7	39.2 \pm 4.5	135.0 \pm 2.3	120.6 \pm 2.6	305.8 \pm 1.2



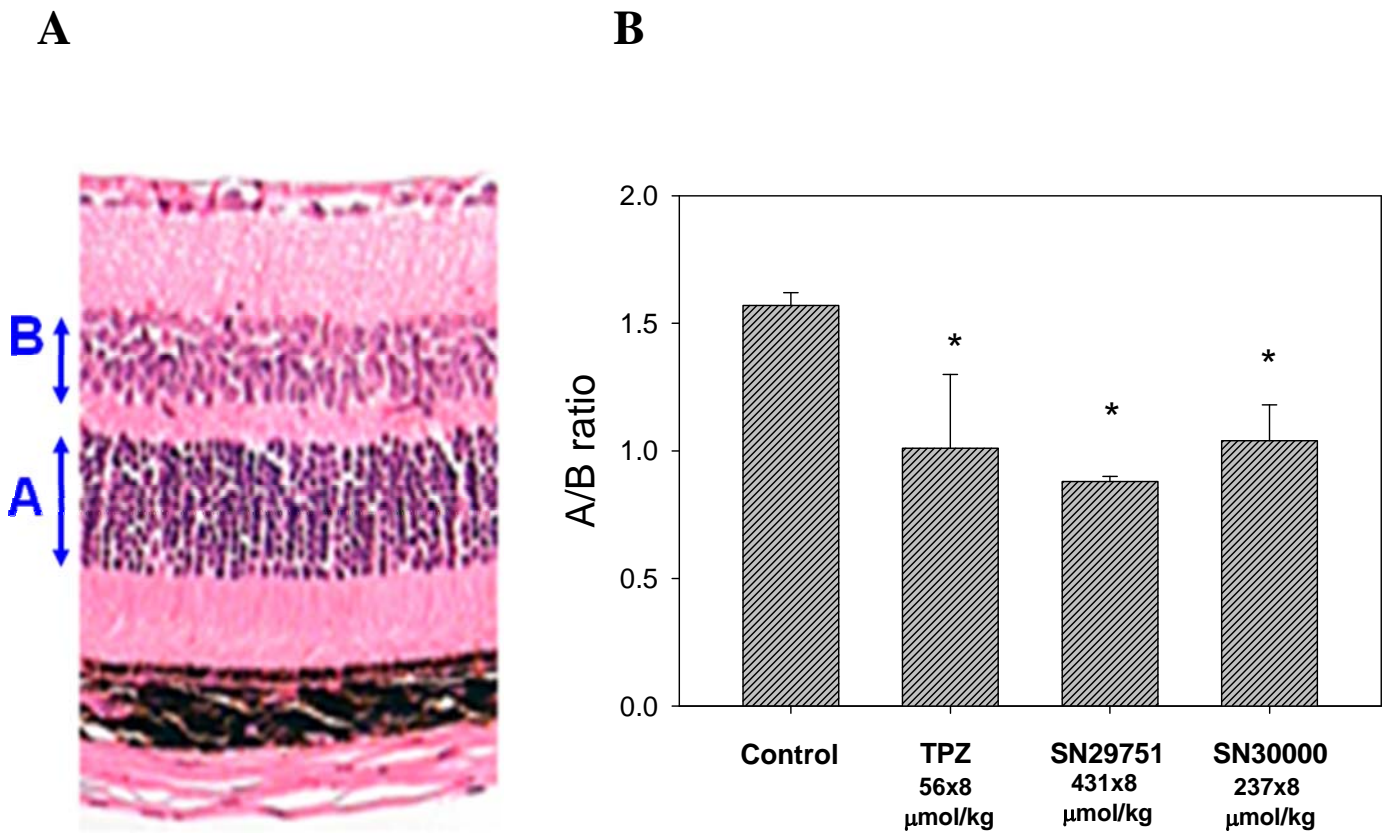
Supplementary Fig S1: Representative HPLC chromatogram of extracellular medium from an experiment in which HT29 cells suspensions (10^6 /ml) were exposed to SN30000 under hypoxia (0% oxygen in the gas phase) to provide the time course data in Fig 1D. The above sample was analysed 3 hr after adding SN30000 (initial concentration 40 μ M). The 1-oxide metabolite was identified by comparison of retention time and absorbance spectrum (insert) with synthetic 1-oxide.



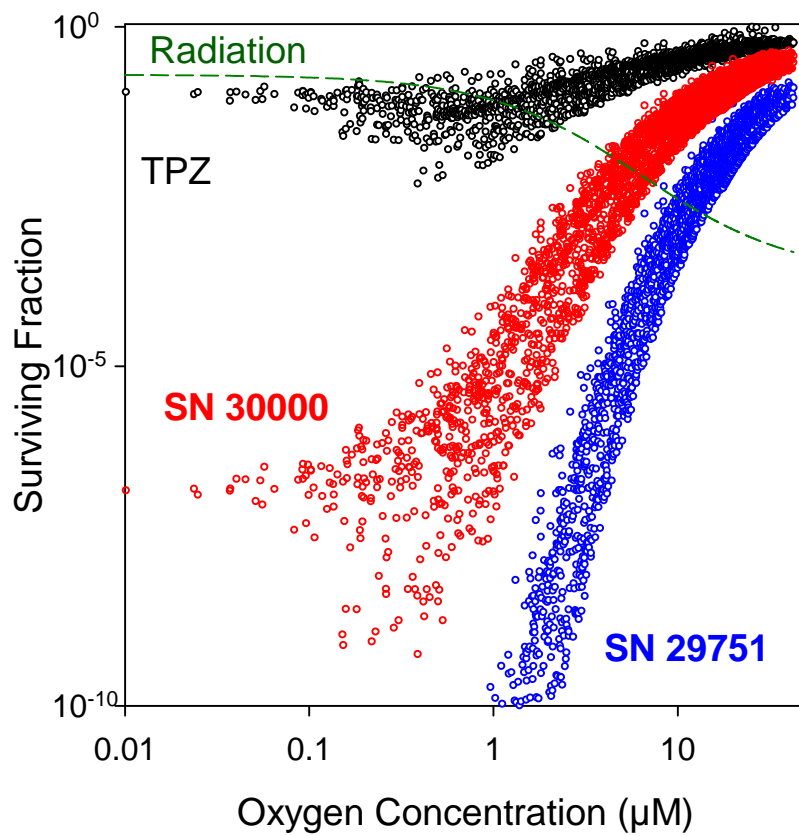
Supplementary Fig S2: Flux of TPZ (grey symbols), SN29751 (open symbols) and SN 30000 (black, filled symbols) through SiHa MCL. The ordinate is the concentration in the receiver compartment normalised to the expected concentration at infinite time and plotted against normalised flux of the ^{14}C -urea internal standard instead of time to account for differences in MCL thickness. Two replicate experiments are shown for each compound.



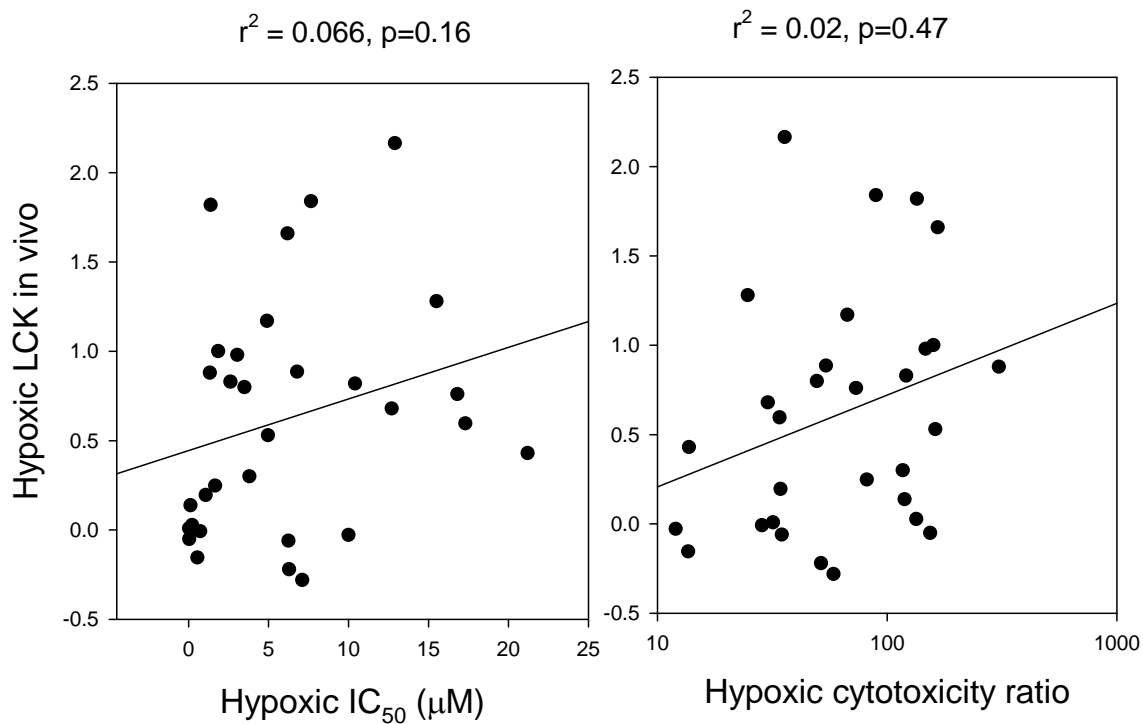
Supplementary Fig S3: Oxygen dependence of the rate constant for metabolic consumption of SN29751 and SN30000, normalized to the rate constant under anoxia. Curves are model fits with the K-value for metabolism (oxygen concentration for 50% inhibition) as the fitted parameter (Dotted line: SN29751; Solid line: SN30000).



Supplementary Fig S4: Retinal toxicity of TPZ and analogues in CD-1 nude mice. A: histology of a control CD-1 nude mouse retina (formalin fixed paraffin embedded section, H&E stain). The thickness of the outer and inner nuclear layers (A and B respectively) were measured at 20 points along the length of each retina, using a 40× objective and eyepiece graticule, essentially as described by Lee and Wilson, *Toxicol Appl Pharmacol* 163: 50-59, 2000. B: Selective loss of the outer nuclear layer (decrease in ratio A/B) in retina 28 days after the start of dosing with TPZ and analogs (BID1-4) at their respective MTD. Values are mean and SEM for 2-4 (treated) or 9 (control) mice. * signifies significantly different from control ($p < 0.05$) by one way ANOVA and the Holm-Sidak method.



Supplementary Fig S5: Predictions of the SR-PKPD model for cell killing in HT29 tumors (plotted as a function of oxygen concentration at each position in the microvascular network), based on plasma PK input in male Sprague-Dawley rats after i.p. dosing at the MTD (plasma PK data from Figure 4B).



Supplementary Fig S6: Lack of correlation of potency (IC₅₀) or hypoxic cytotoxicity ratio (HCR) with hypoxic log cell kill (LCK) *in vivo*. The plots include all compounds that were tested in the HT29 xenograft excision assay during the analog development program. Note that the more potent compounds tend to show lower LCK *in vivo*.